Supporting Information

Ligand-controlled exposure of active sites on Pd_1Ag_{14} nanoclusters surface to boost electrocatalytic CO_2 reduction

Along Ma,[a,b] Yonggang Ren,[b] Yang Zuo,[b] Jiawei Wang,[b] Shutong Huang,[b] Xiaoshuang Ma[b] and Shuxin Wang *[a,b]

[a]*Shandong Key Laboratory of Biochemical Analysis, College of Chemistry and Molecular Engineering, Qingdao University of Science and Technology, Qingdao 266042, P. R. China*.

[b]*College of Materials Science and Engineering, Qingdao University of Science and Technology, Qingdao 266042, P. R. China.*

*Corresponding authors. E-mail: shuxin_wang@qust.edu.cn

Notes: The authors declare no competing financial interest.

Table of Contents

Section 3. Supporting Table

Section 1. Experimental procedures

I. Synthesis

Chemicals: All reagents were commercially available and used without further purification. Palladium (II) acetylacetonate ($C_{10}H_{14}O_4Pd$, 99% metal basis), silver acetate (CH_3COOAg, 98% metals basis), phenyl mercaptan (PhSH, 99%), 3,5-bis(trifluoromethyl)thiophenol ($(CF_3)_2PhSH$, 99%), triphenylphosphine (PPh_3, 98.8%), tris(4-methoxyphenyl)phosphine ($P(Ph\text{-}p\text{-}OMe)_3$, 98%), sodium borohydride ($NaBH_4$, 98%), cesium acetate (CH_3COOCs, 98%), methyl alcohol (CH_3OH, HPLC grade), ethyl alcohol (CH_3CH_2OH, HPLC grade), dichloromethane (CH_2Cl_2, HPLC grade), acetonitrile (CH_3CN, HPLC grade) and n-hexane (Hex, HPLC grade), were used to carry out the experiments. All glassware was thoroughly cleaned with aqua regia ($V_{HCl} : V_{HNO3}$ = 3:1), rinsed with copious pure water, and then dried in an oven prior to use.

Synthesis of $Pd_1Ag_{14}(PPh_3)_8(SPh(CF_3)_2)_6$ (Pd_1Ag_{14}-S) nanocluster: The reaction was conducted in an ice bath. Typically, $C_{10}H_{14}O_4Pd$ (6 mg, 0.020 mmol) and CH_3COOAg (50 mg, 0.3 mmol, dissolved in 1 mL of H_2O) were added to a mixture of 10 mL CH_3CH_2OH and 10 mL CH_2Cl_2 under vigorous stirring. After stirring for 5 minutes, PPh_3 (200 mg, 0.76 mmol) and $(CF_3)_2PhSH$ (162 μL, 0.96 mmol) were introduced to the mixture. The reaction solution turned colorless and transparent after 30 minutes. Subsequently, a freshly prepared solution of $NaBH_4$ (42 mg, 1.1 mmol, dissolved in 2 mL of H_2O) was added, causing the solution to gradually darken. The reaction proceeded for 12 hours, yielding the **$Pd_1Ag_{14}(PPh_3)_8(SPh(CF_3)_2)_6$** nanocluster with an approximate 23% yield (based on Ag atom). The crude product was washed three times with CH_3OH to remove by-products. Dark red, block-shaped crystals were obtained by crystallizing the purified nanoclusters in DCM/Hex (1 : 3) system at 4°C over 4 days.

Synthesis of $Pd_1Ag_{14}(P(Ph\text{-}p\text{-}OMe)_3)_7(SPh)_6$ (Pd_1Ag_{14}-E) nanocluster: The **Pd_1Ag_{14}-E** nanocluster was synthesized utilizing a methodology similar to that used for the **Pd_1Ag_{14}-S** nanocluster. The molar ratio of $P(Ph\text{-}p\text{-}OMe)_3$ used was equivalent to that of the PPh_3 ligand in the **Pd_1Ag_{14}-S** synthesis, and the molar ratio of PhSH was maintained identical to that of the $(CF_3)_2PhSH$ ligand. Detailedly, $C_{10}H_{14}O_4Pd$ (6 mg, 0.020 mmol) and CH_3COOAg (50 mg, 0.3 mmol, dissolved in 1 mL of H_2O) were added to a mixture of 10 mL CH_3CH_2OH and 10 mL CH_2Cl_2 under vigorous stirring. After stirring for 5 minutes, $P(Ph\text{-}p\text{-}OMe)_3$ (268 mg, 0.76 mmol) and PhSH (99 μL, 0.96 mmol) were introduced. The reaction solution transitioned light red and transparent after 30 minutes. Successively, a freshly prepared solution of $NaBH_4$ (42 mg, 1.1 mmol, dissolved in 2 mL of H_2O) was added, causing the solution to gradually darken. The reaction was maintained for 12 hours, yielding the **$Pd_1Ag_{14}(P(Ph\text{-}p\text{-}OMe)_3)_7(SPh)_6$** nanocluster with an approximate 15% yield (based on Ag atom). Post-synthesis, the crude product was subjected to three washes with CH_3OH to remove impurities. Finally, dark red, block-shaped crystals were obtained from the purified nanoclusters by crystallization in a DCM/Hex (1 : 3) mixture at 4°C over a period of 4 days.

Conversion from $Pd_1Ag_{14}(PPh_3)_8(SPh(CF_3)_2)_6$ (Pd_1Ag_{14}-S) to Pd_1Ag_{14}-S*. The **Pd_1Ag_{14}-S** (10 mg, 0.00193 mmol) single crystals were dissolved in 15 mL of CH_2Cl_2. Then $P(Ph\text{-}p\text{-}OMe)_3$ (5.44 mg, 0.0154 mmol) and PhSH (1.2 μL, 0.0116 mmol) ligands were dissolved in 1 mL of CH_2Cl_2 and added to reaction under vigorous stirring. After about 8 min, **Pd_1Ag_{14}-S** nanoclusters were converted into the **Pd_1Ag_{14}-S*** nanoclusters, then massive CH_3CN was added to stop the reaction. To acquire the pure **Pd_1Ag_{14}-S***, the crude product was washed two times with CH_2Cl_2/CH_3OH (1 : 10) to remove excess mercaptan and phosphine ligands (yield ~90 %, Ag atom basis). The solid powder of **Pd_1Ag_{14}-S*** was stored in the refrigerator and kept in reserve.

II. Characterization

Ultraviolet-visible spectroscopy (**UV-vis**): The UV-vis measurements in this study were recorded on a Shanghai Metash UV-8000 spectrophotometer. All samples were dissolved in CH_2Cl_2 for spectrum measurements.

X-ray photoelectron spectroscopy (**XPS**): The XPS measurements were performed on ESCALAB XI+ configured with a monochromated $Al_{K\alpha}$ (1486.8 eV) 150W X-ray source, 0.5 mm circular spot size, a flood gun to counter charging effects, and the analysis chamber base pressure lower than 1 $x10^{-9}$ mbar, data were collected with FAT = 20 eV. The crystal particles of **Pd_1Ag_{14}-S** and **Pd_1Ag_{14}-E** were tested by sticking on packaging tape for testing. And the **Pd_1Ag_{14}-S*** pure product was dissolved in CH_2Cl_2 to form a concentrated solution and then applied to the surface of packaging tape for testing. Then, a small amount of carbon was added to help with the data correction.

Scanning electron microscope-energy dispersive spectrometer (**SEM-EDS**): SEM-EDS was conducted on JSM-6700F. The crystal particles of **Pd_1Ag_{14}-S** and **Pd_1Ag_{14}-E** were tested by sticking on a conductive adhesive with an accelerating voltage of 0.1-30 kV. And the **Pd_1Ag_{14}-S*** pure product was dissolved in CH_2Cl_2 to form a concentrated solution and then applied to the surface of silicon wafers for testing.

Thermogravimetric analysis (**TGA**): TGA was carried out on a thermogravimetric analyzer (DTG-60H) with ~8 mg of nanoclusters in a SiO_2 pan at a heating rate of 20 K/min under an N_2 atmosphere. And the sample was extracted for 4 hours to remove the solvent molecules using a vacuum pump, before TGA testing.

Nuclear magnetic resonance (**NMR**): NMR measurements were performed using a Bruker Avance spectrometer operating at 400 MHz for ^1H. For the preparation sample, after 400 μL of the cathode reaction solution and 200 μL of D_2O (using DMSO as an internal standard) were mixed, ^1H NMR tests were performed directly.

Electrospray ionization mass spectrometry (**ESI-MS**): ESI-MS measurements were carried out on a Bruker micro TOF-Q system in positive or negative ion mode in the range m/z = 1000-10000. To prepare the ESI sample, clusters were dissolved in CH_2Cl_2/CH_3OH (V/V = 1 : 3) and diluted in the same solvent to a concentration of approximately 100 ppm and the molar ratio of clusters to CH_3COOCs is 1 : 30.

Matrix-assisted laser desorption ionization-time of flight mass spectrometry (**MALDI-TOF-MS**): MALDI-MS was performed on a Bruker Microflex LRF. Trans-2-[3-(4-tert-butylphenyl)-2-methyl-2-propenyldidene]-malononitrile (DCTB) was used as the matrix with a 1 : 500 analyte matrix ratio and dissolved in CH_2Cl_2. A volume of 3 μL of the analyte matrix mixture was applied to the target and air-dried.

X-ray crystallography: The data collections for single crystal X-ray diffraction (SC-XRD) were carried out on a Bruker D8 Quest at 170 K, using a Mo-Kα radiation (λ = 0.71073 Å). The structure was solved by intrinsic phasing and refined with full-matrix least squares on F^2 using the SHELXTL software package. All non-hydrogen atoms were refined anisotropically, and all the hydrogen atoms were set in geometrically calculated positions and refined isotopically using a riding model. Detailed crystal data for **Pd_1Ag_{14}-S** and **Pd_1Ag_{14}-E** nanoclusters are given in Table S1 and S2, respectively. CCDC 2324593 for **Pd_1Ag_{14}-S** and CCDC 2324594 for **Pd_1Ag_{14}-E** contain the supplementary crystallographic data for this paper. These data are provided free of charge by the Cambridge Crystallographic Data Centre.

III. Electrochemical measurements

To prepare the catalyst sample, the as-prepared **Pd_1Ag_{14}** nanoclusters were loading on Ketjen Carbon (C) with a mass ratio of 1 (5 mg nanoclusters and 5 mg Ketjen Carbon). The catalyst ink was prepared by dispersing the sample in isopropanol (2.5 mg·mL^{-1}) under sonication for 20 minutes. Then, 1 mL catalyst suspension and 10 μL Nafion (5 wt.%) were uniformly mixed as the final catalyst ink. Subsequently, 40 μL catalytic ink was dropwise cast onto the carbon cloth (1 × 1 cm^2) and dried at room temperature as the working electrode. 0.5 M $KHCO_3$ solution (pH = 7.2 when saturated with CO_2) was used as the electrolyte.

The electrochemical properties of three catalysts were evaluated on a CHI 760E electrochemical workstation. All electrochemical measurements were carried out in a custom gas-tight H-cell with two compartments separated by Nafion 117 membrane. Each compartment contained 25 mL electrolyte (0.5 M $KHCO_3$) with approximately 10 mL headspace. Ag/AgCl in 0.5 M $KHCO_3$ saturated aqueous electrolyte was employed as the reference electrode. Electrode potentials measured on the Ag/AgCl scale ($E_{Ag/AgCl}$) were converted into the reversible hydrogen electrode (RHE) scale using the following equation:

$$E(RHE) = E(Ag/AgCl) + 0.1976 + 0.0592 * pH$$

The output of the gas flow from the cathode chamber passes through a gas flow controller (the gas flow controller was used to control the gas flow rate) and then into a gas chromatograph instrument (GC3900Plus, RUI NENG) for on-line identification and quantification of the gaseous products, which was purged for 30 min with an average rate of 10 mL·min^{-1} (at room temperature and ambient pressure) prior to the test.

The faradaic efficiency (FE_X) and partial current density (j_X) of X (X= CO or H_2) were calculated as below:

$$FE_X = \frac{(N_i \times n \times F)}{Q_t}$$

$$j_X = \frac{FE_X \times Q_t}{t \times \text{Area}}$$

Where

Q_t = total charge consumed in the electrochemical reaction

N_i = the number of moles of the product (measured GC)

n = the number of electrons transferred in the elementary reaction (n is 2 for CO and H_2)

F = the Faradaic constant (96485 C mol^{-1})

t = reaction time (s)

Area = geometry area of the electrode (1 cm^2)

After the eCO_2RR tests were completed, the samples were rinsed with CH_2Cl_2 and collected for UV-vis characterization.

Section 2. Supporting Figures

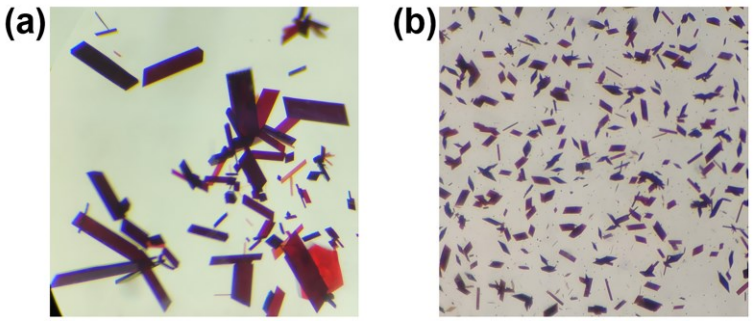

Fig. S1 The optical microscopic image of the single crystals of **Pd_1Ag_{14}-S** and **Pd_1Ag_{14}-E** nanoclusters. (a) **Pd_1Ag_{14}-S**; (b) **Pd_1Ag_{14}-E**.

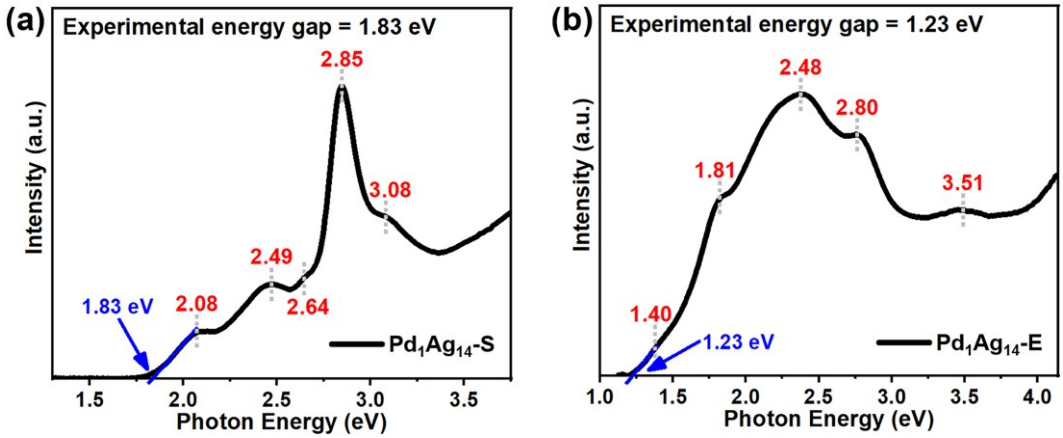

Fig. S2 UV-vis absorption spectra (photon energy scale) of the **Pd_1Ag_{14}-S** and **Pd_1Ag_{14}-E** nanoclusters in CH_2Cl_2. (a) **Pd_1Ag_{14}-S**; (b) **Pd_1Ag_{14}-E**. The experimental energy gap of the **Pd_1Ag_{14}-S** and **Pd_1Ag_{14}-E** nanoclusters in CH_2Cl_2 was determined as ~1.83 eV and 1.23 eV, respectively.

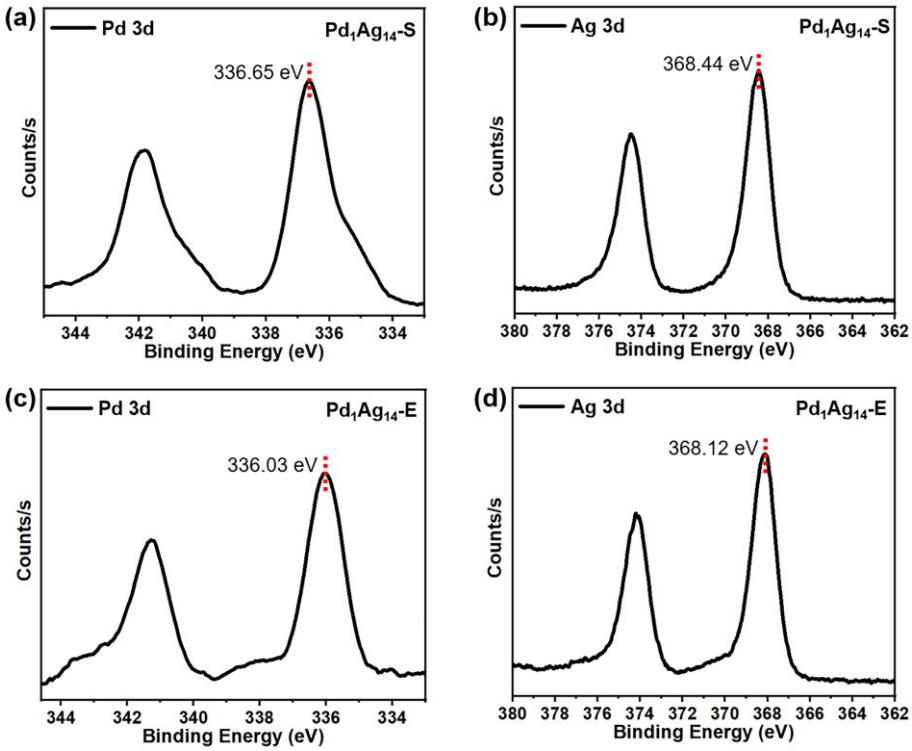

Fig. S3 XPS spectra of the **Pd_1Ag_{14}-S** and **Pd_1Ag_{14}-E** nanoclusters. (a) Pd 3d of the **Pd_1Ag_{14}-S**; (b) Ag 3d of the **Pd_1Ag_{14}-S**; (c) Pd 3d of the **Pd_1Ag_{14}-E**; (d) Ag 3d of the **Pd_1Ag_{14}-E**.

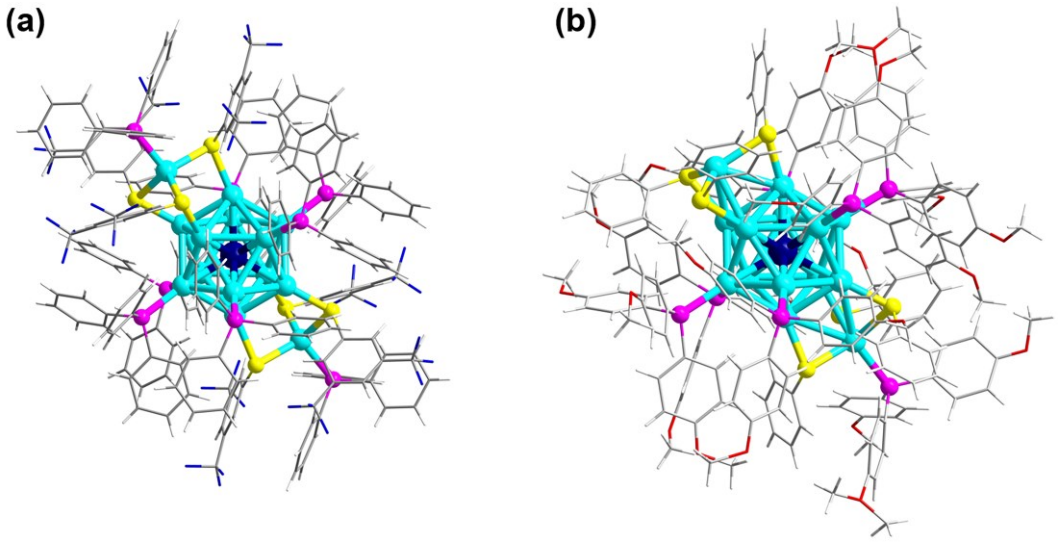

Fig. S4 The overall structure of the **Pd_1Ag_{14}-S** and **Pd_1Ag_{14}-E** nanoclusters. (a) **Pd_1Ag_{14}-S**; (b) **Pd_1Ag_{14}-E**. Color labels: dark blue = Pd; light blue = Ag; yellow = S; magenta = P; blue = F; red = O; grey = C; white = H.

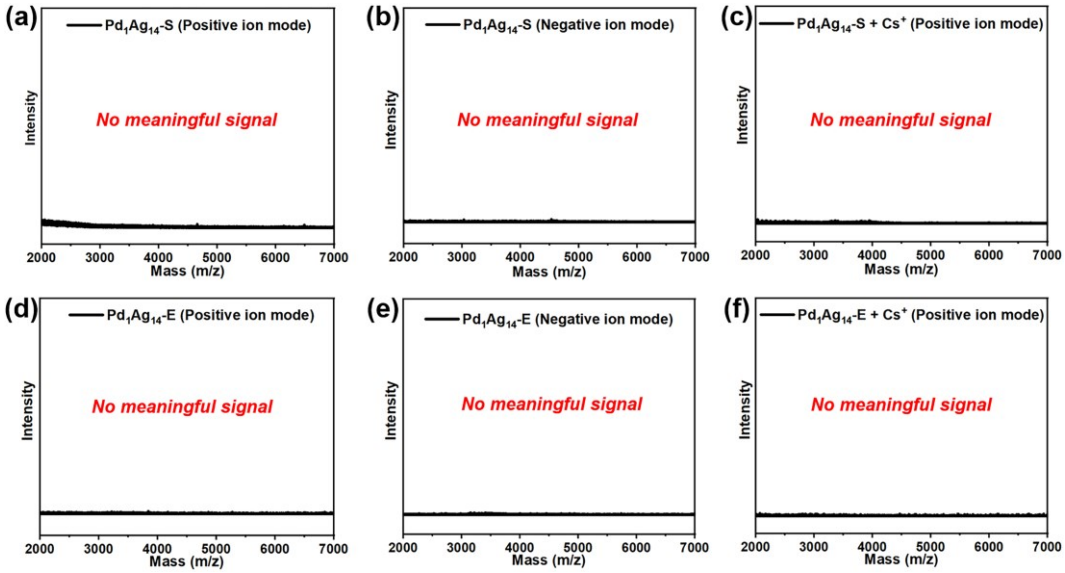

Fig. S5 ESI-MS spectra of **Pd_1Ag_{14}-S** and **Pd_1Ag_{14}-E** nanoclusters. (a) and (d) Positive ion mode; (b) and (e) Negative ion mode; (c) and (f) Positive ion mode with the addition of Cs^+.

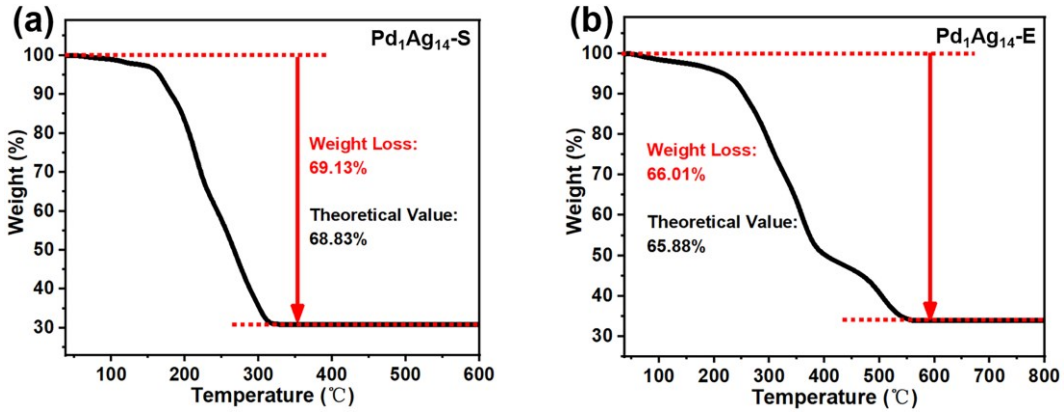

Fig. S6 TGA spectra of the **Pd_1Ag_{14}-S** and **Pd_1Ag_{14}-E** nanoclusters. (a) **Pd_1Ag_{14}-S**; (b) **Pd_1Ag_{14}-E**.

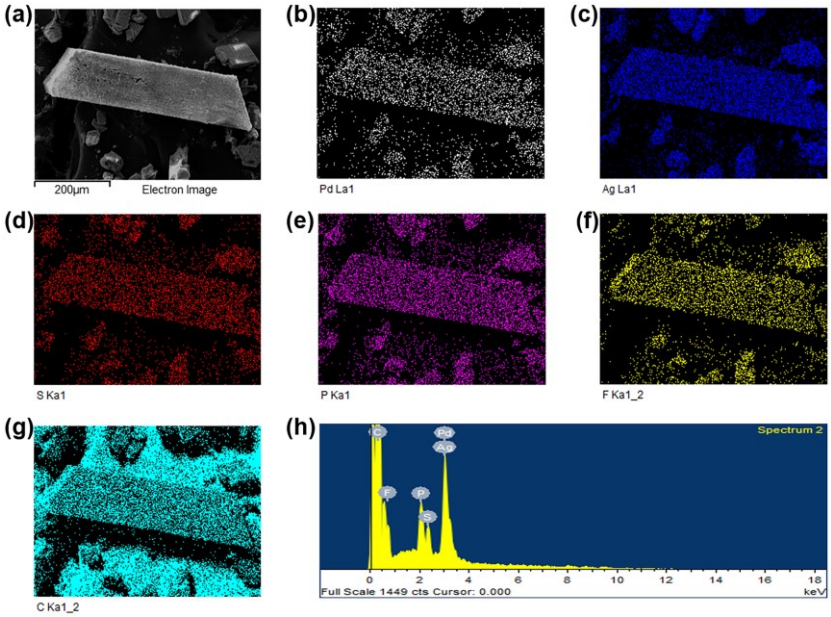

Fig. S7 SEM image and corresponding elemental mapping images of the **Pd_1Ag_{14}-S** nanocluster. (a) SEM image of single crystal; (b)-(g) Elemental mapping images of Pd, Ag, S, P, F and C elements, respectively; (h) EDS spectrum confirming the presence of above elements (Pd, Ag, S, P, F and C) in **Pd_1Ag_{14}-S** nanocluster, which is consistent with the cluster composition obtained by SC-XRD.

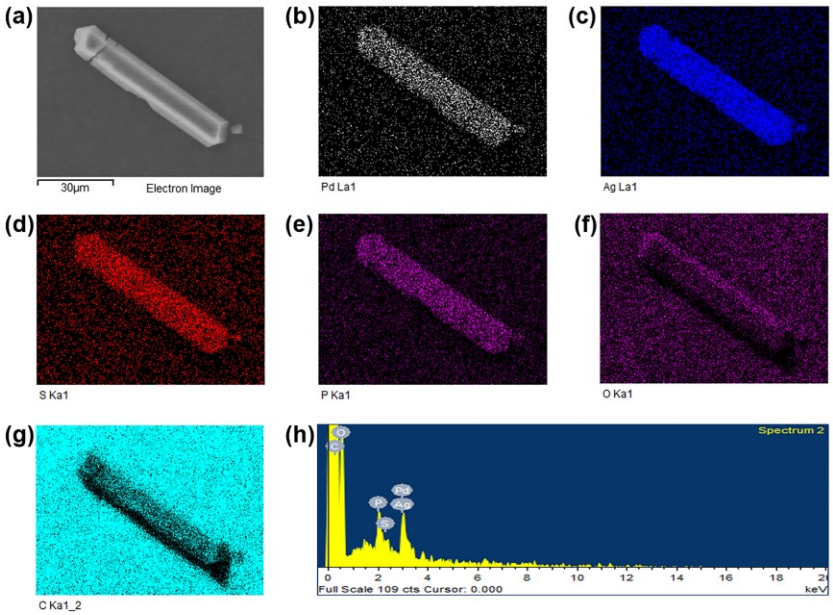

Fig. S8 SEM image and corresponding elemental mapping images of the **Pd_1Ag_{14}-E** nanocluster. (a) SEM image of single crystal; (b)-(g) Elemental mapping images of Pd, Ag, S, P, O and C elements, respectively; (h) EDS spectrum confirming the presence of above elements (Pd, Ag, S, P, O and C) in **Pd_1Ag_{14}-E** nanocluster, which is consistent with the cluster composition obtained by SC-XRD.

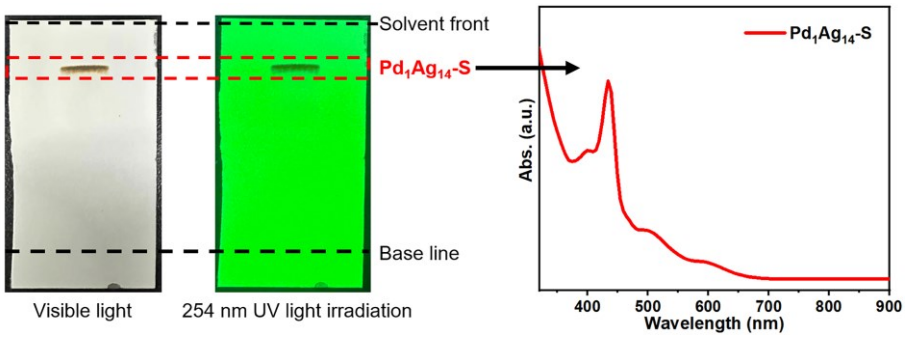

Fig. S9 Photographs of crystals of **Pd_1Ag_{14}-S** was separated using PTLC, and the corresponding UV was shown. Solvent system: the volume ratio of CH_2Cl_2 and Hex is 1 : 1.

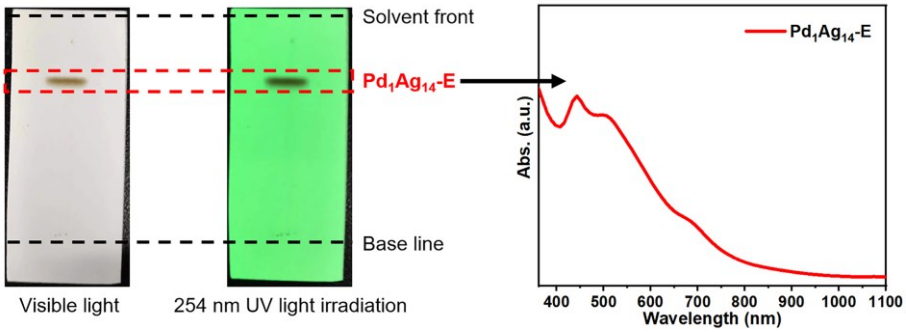

Fig. S10 Photographs of crystals of **Pd_1Ag_{14}-E** was separated using PTLC, and the corresponding UV was shown. Solvent system: the volume ratio of CH_2Cl_2 and Hex is 1.5 : 1.

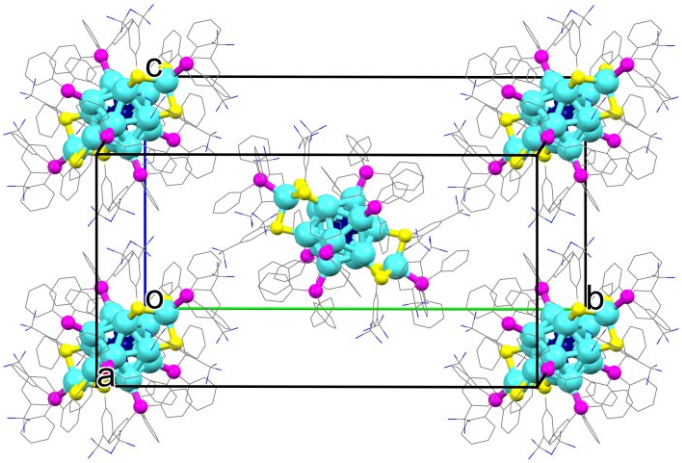

Fig. S11 A unit cell in the **Pd_1Ag_{14}-S** single crystal. Color labels: dark blue = Pd; light blue = Ag; yellow = S; magenta = P; blue = F; grey = C. All H atoms are omitted for clarity.

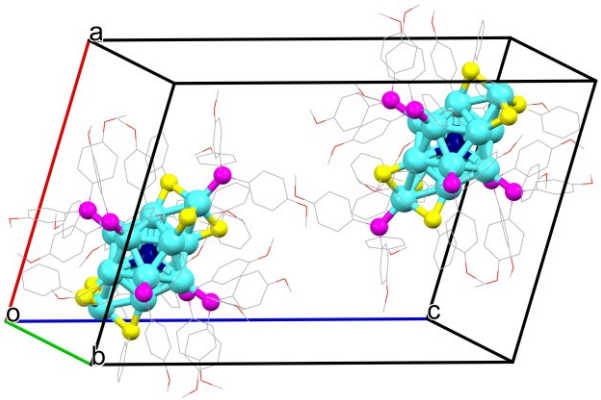

Fig. S12 A unit cell in the **Pd_1Ag_{14}-E** single crystal. Color labels: dark blue = Pd; light blue = Ag; yellow = S; magenta = P; red = O; grey = C. All H atoms are omitted for clarity.

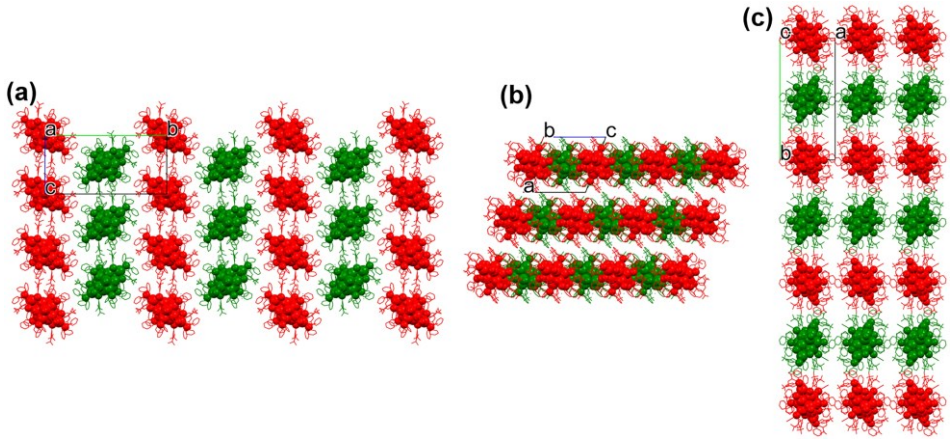

Fig. S13 Packing mode of **Pd_1Ag_{14}-S** in the crystal shown. (a) Along the a axis; (b) along the b axis; (c) along the c axis. All H atoms are omitted for clarity. The cluster molecules arranged in different directions show in different colors.

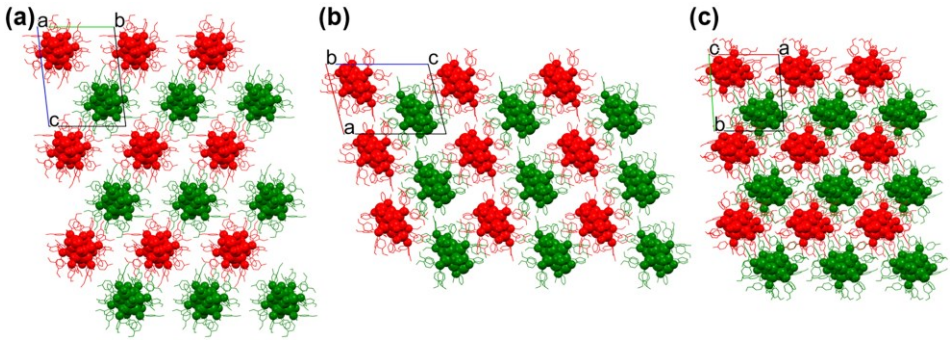

Fig. S14 Packing mode of **Pd_1Ag_{14}-E** in the crystal shown. (a) Along the a axis; (b) along the b axis; (c) along the c axis. All H atoms are omitted for clarity. The cluster molecules arranged in different directions show in different colors.

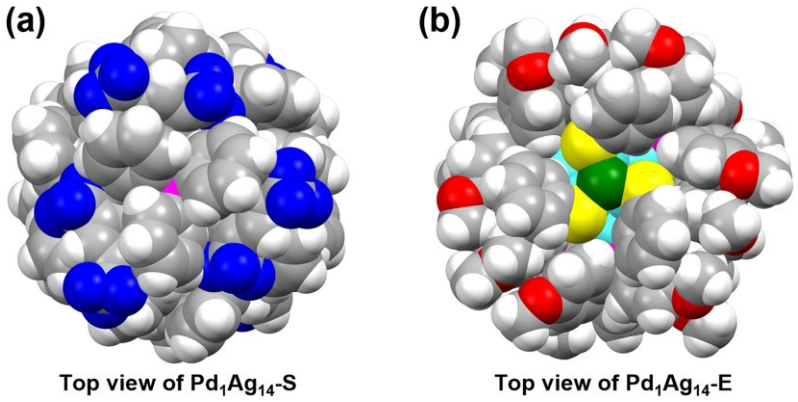

Fig. S15 Top view of the **Pd_1Ag_{14}-S** and **Pd_1Ag_{14}-E** nanoclusters. (a) **Pd_1Ag_{14}-S**; (b) **Pd_1Ag_{14}-E**. Color labels: dark blue = Pd; light blue = $Ag_{icosahedral\ surface}$; green = Ag_{shell}; yellow = S; magenta = P; blue = F; red = O; grey = C; white = H.

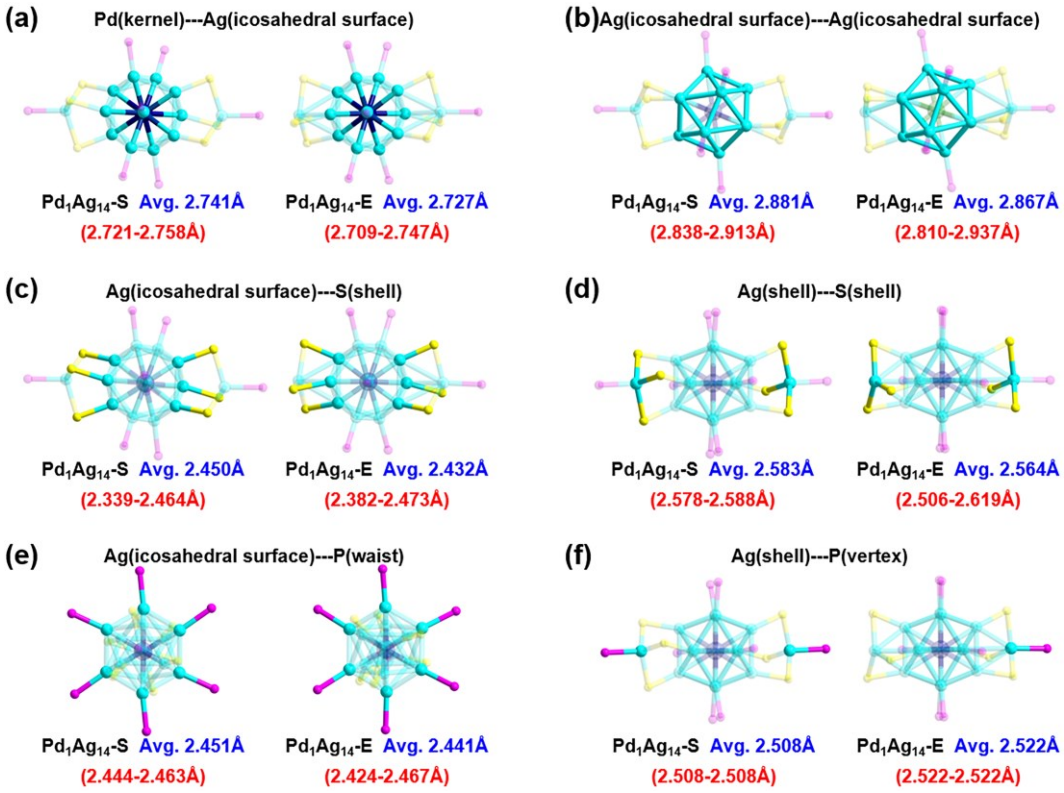

Fig. S16 Structural comparison and bond length among **Pd_1Ag_{14}-S** and **Pd_1Ag_{14}-E** nanoclusters. (a) Comparison of the bond length of Pd(kernel)---Ag(icosahedral surface); (b) Comparison of the bond length of Ag(icosahedral surface)---Ag(icosahedral surface); (c) Comparison of the bond length of Ag(icosahedral surface)---S(shell); (d) Comparison of the bond length of Ag(shell)---S(shell); (e) Comparison of the bond length of Ag(icosahedral surface)---P(waist); (f) Comparison of the bond length of Ag(shell)---P(vertex). The compared bonds are highlighted in solid. Color labels: dark blue = Pd; light blue = Ag; yellow = S; magenta = P.

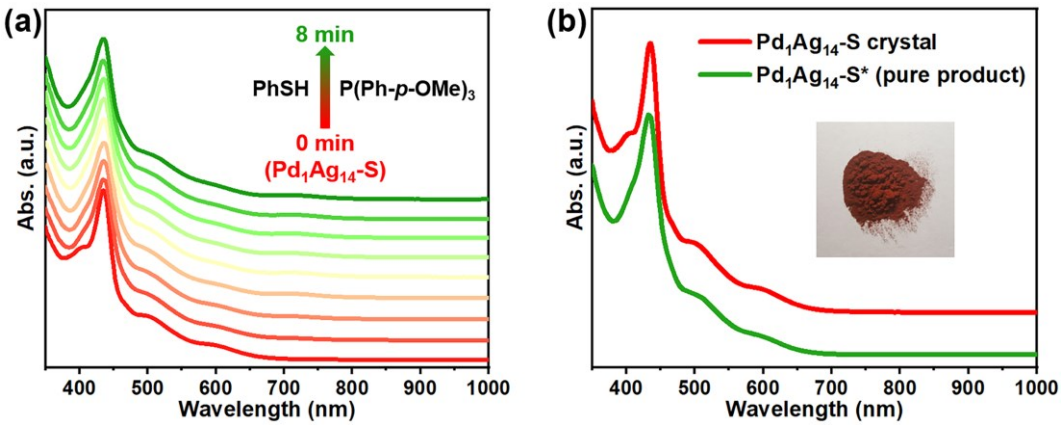

Fig. S17 (a) The UV-vis spectra of the conversion from **Pd_1Ag_{14}-S** to **Pd_1Ag_{14}-S***; (b) The UV-vis spectra of **Pd_1Ag_{14}-S** crystal (red line) and **Pd_1Ag_{14}-S*** pure product (green line) in CH_2Cl_2 (Inset: the photograph of **Pd_1Ag_{14}-S*** solid powder).

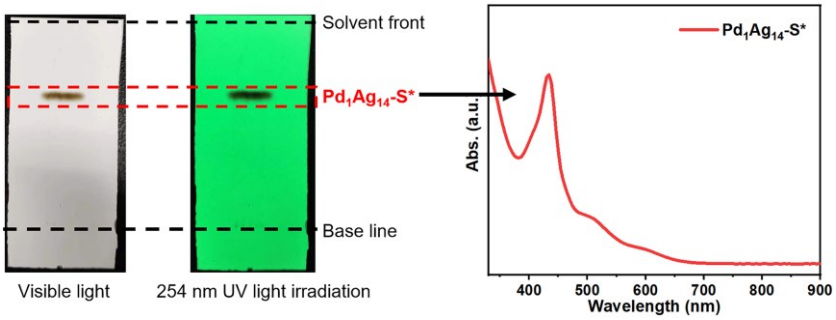

Fig. S18 Photographs of crystals of **Pd_1Ag_{14}-S*** was separated using PTLC, and the corresponding UV was shown. Solvent system: the volume ratio of CH_2Cl_2 and Hex is 1 : 1.

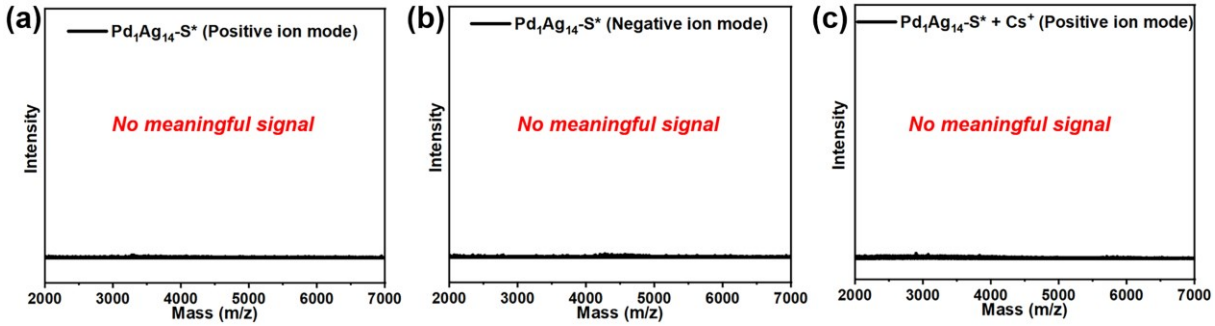

Fig. S19 ESI-MS spectra of **Pd_1Ag_{14}-S*** nanoclusters. (a) Positive ion mode; (b) Negative ion mode; (c) Positive ion mode with the addition of Cs^+.

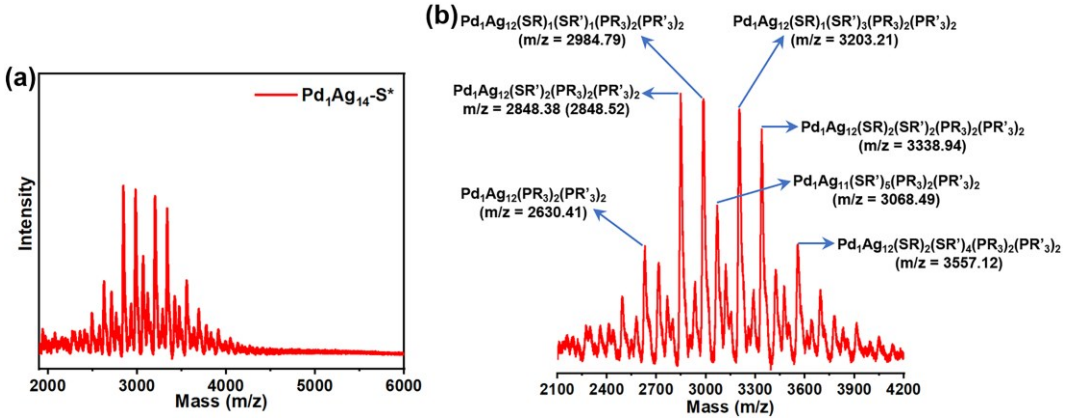

Fig. S20 (a) MALDI mass spectrum of **Pd_1Ag_{14}-S*** nanoclusters. (b) MALDI mass spectrum of **Pd_1Ag_{14}-S*** nanoclusters from 2100 Da to 4200 Da in Figure S20a, and detailed species analysis. (SR = $SPh(CF_3)_2$; PR_3 = PPh_3; SR' = SPh; PR'$_3$ = P(Ph-*p*-OMe)$_3$).

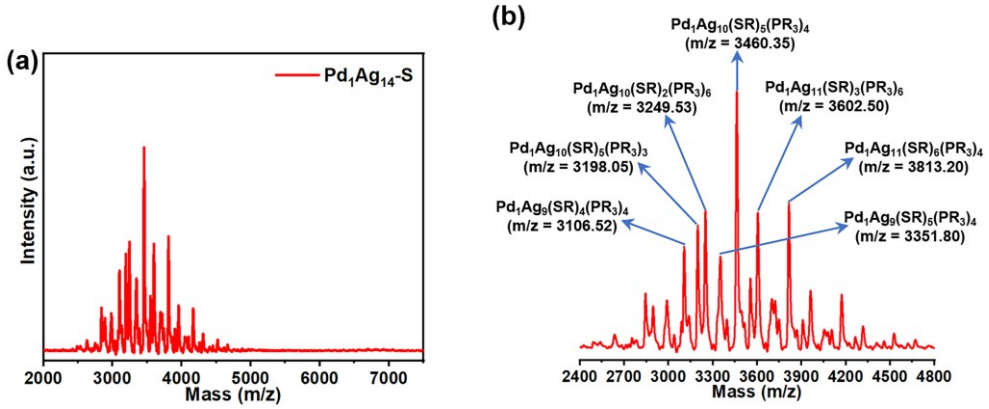

Fig. S21 (a) MALDI mass spectrum of **Pd_1Ag_{14}-S** nanoclusters. (b) MALDI mass spectrum of **Pd_1Ag_{14}-S** nanoclusters from 2400 Da to 4800 Da in Figure S21a, and detailed species analysis. (SR = $SPh(CF_3)_2$; PR_3 = PPh_3).

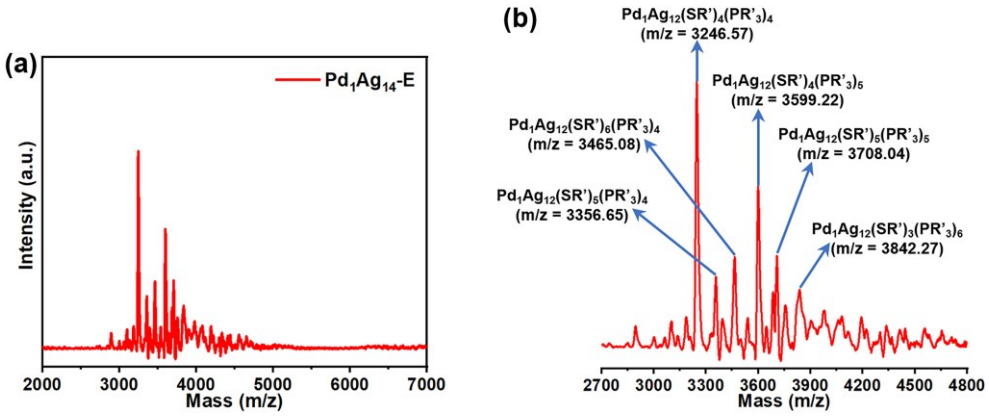

Fig. S22 (a) MALDI mass spectrum of **Pd_1Ag_{14}-E** nanoclusters. (b) MALDI mass spectrum of **Pd_1Ag_{14}-E** nanoclusters from 2700 Da to 4800 Da in Figure S22a, and detailed species analysis. (SR' = SPh; PR'$_3$ = P(Ph-*p*-OMe)$_3$).

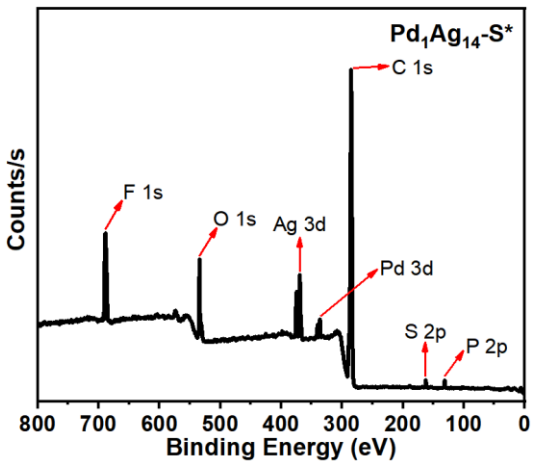

Fig. S23 XPS spectrum of the **Pd_1Ag_{14}-S*** nanoclusters. XPS result (Fig. S23, Table S3 and Table S4) showed an Ag/ F/ O ratio of 14/ 19.3/ 12.7 based on Ag atom, implying the replacement of approximately 2.8 SR (calculated as 6(F) × 6(SR) - 19.3(F) = 16.7(F) ≈ 6(F) × 2.8(SR)) ligands with SR' and about 4.2 PR_3 (calculated as 12.7(O) ≈ 3(O) × 4.2(PR'_3)) ligands with PR'_3.

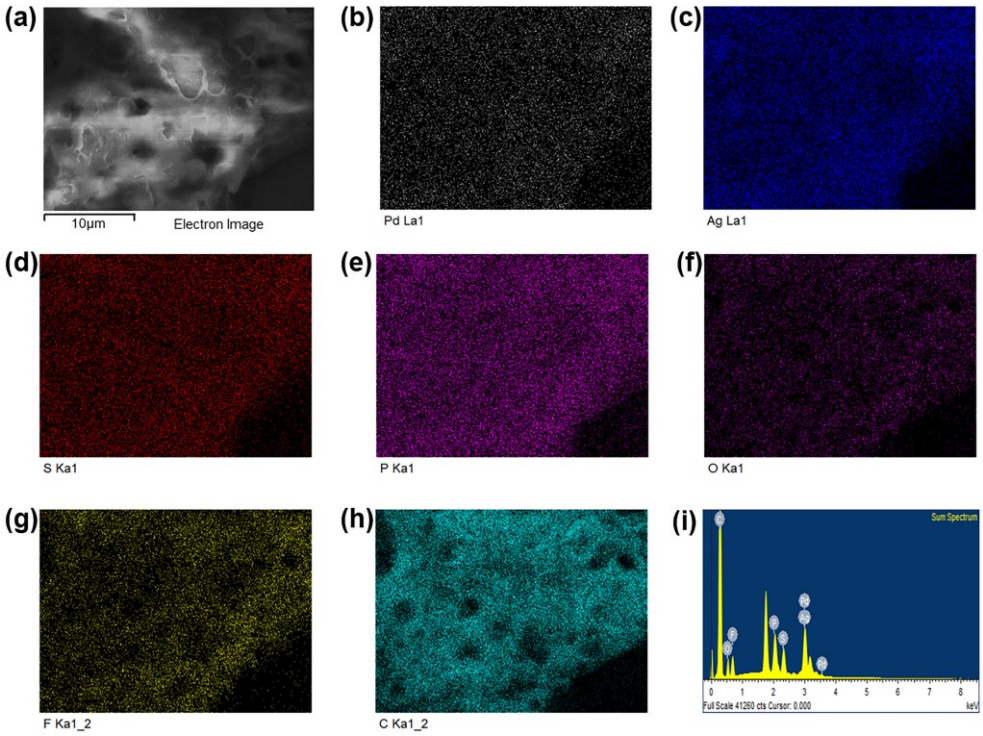

Fig. S24 SEM image and corresponding elemental mapping images of the **Pd_1Ag_{14}-S*** nanocluster. (a) SEM image of solid product; (b)-(h) Elemental mapping images of Pd, Ag, S, P, O, F and C elements, respectively; (f) EDS spectrum confirming the presence of above elements (Pd, Ag, S, P, O, F and C) in **Pd_1Ag_{14}-S*** nanocluster. EDS result (Fig. S24, Table S3 and Table S4) displayed an Ag/ F/ O ratio of 14/ 15.7/ 11.2, indicating the substitution of about 3.4 SR (calculated as 6(F) × 6(SR) - 15.7(F) = 20.3(F) ≈ 6(F) × 3.4(SR)) and 3.7 PR_3 (calculated as 11.2(O) ≈ 3(O) × 3.7(PR'_3)) ligands with SR' and PR'_3, respectively.

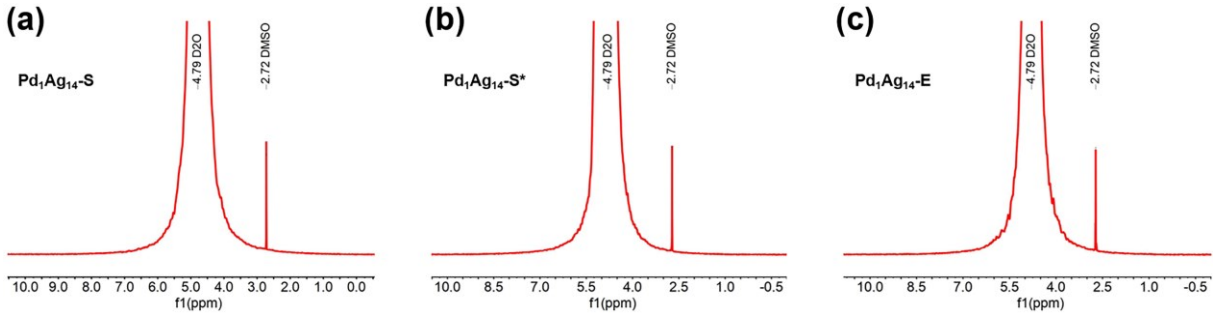

Fig. S25 The ^{1}H NMR spectra of the catholyte reaction solution for **Pd_1Ag_{14}-S/C**, **Pd_1Ag_{14}-S*/C** and **Pd_1Ag_{14}-E/C**. (a) **Pd_1Ag_{14}-S/C**; (b) **Pd_1Ag_{14}-S*/C**; (c) **Pd_1Ag_{14}-E/C**. The spectra demonstrate the absence of any liquid products.

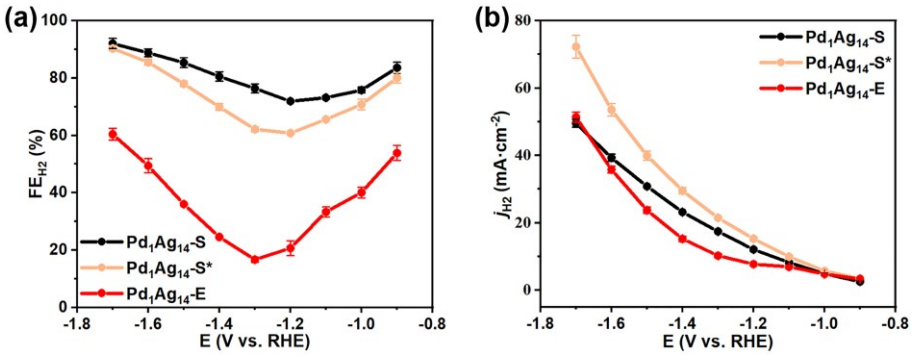

Fig. S26 (a) H_2 faradaic efficiency of the **Pd_1Ag_{14}-S/C** (black), **Pd_1Ag_{14}-S*/C** (tan) and **Pd_1Ag_{14}-E/C** (red) at different potentials. (b) H_2 partial current density of the **Pd_1Ag_{14}-S/C** (black), **Pd_1Ag_{14}-S*/C** (tan) and **Pd_1Ag_{14}-E/C** (red) at different potentials.

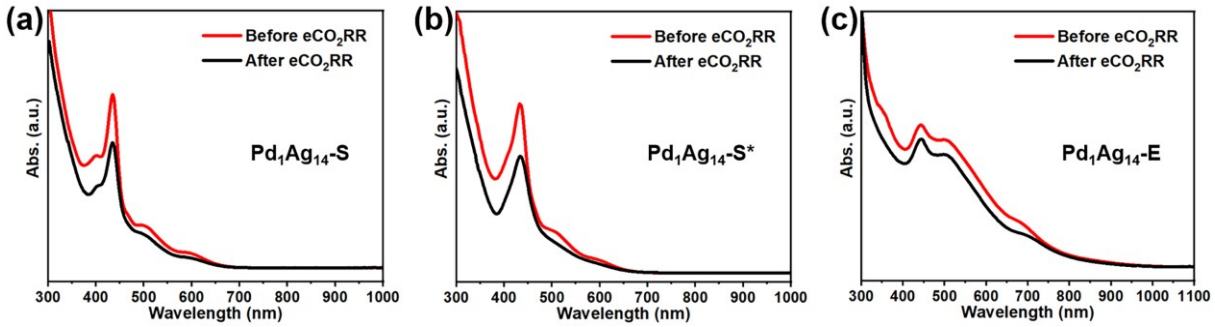

Fig. S27 UV-vis absorbance spectra of the three nanoclusters before and after eCO_2RR. (a) **Pd_1Ag_{14}-S**; (b) **Pd_1Ag_{14}-S***; (c) **Pd_1Ag_{14}-E**.

Section 3. Supporting Table

Table S1 The crystal structure parameters for **$Pd_1Ag_{14}(PPh_3)_8(SPh(CF_3)_2)_6$** (**$Pd_1Ag_{14}$-S**).

Empirical formula	$C_{194}H_{142}Ag_{14}Cl_4F_{36}P_8PdS_6$
Formula weight	5355.57
Temperature/K	170 K
Crystal system	monoclinic
Space group	$P2_1/c$
a/Å	17.460(9)
b/Å	36.131(11)
c/Å	18.471(6)
α/°	90
β/°	110.07(2)
γ/°	90
Volume/Å^3	10945(8)
Z	2
ρ_{calc}g/cm^3	1.625
μ/mm^{-1}	1.541
F(000)	5236.0
Radiation	Mo Kα (λ = 0.71073)
2Θ range for data collection/°	4.116 to 50
Index ranges	$-16 \le h \le 20$, $-42 \le k \le 42$, $-21 \le l \le 21$
Reflections collected	62648
Independent reflections	19235 [R_{int} = 0.0829, R_{sigma} = 0.0869]
Data/restraints/parameters	19235/1082/1006
Goodness-of-fit on F^2	1.073
Final R indexes [I>=2σ (I)]	R_1 = 0.0931, wR_2 = 0.1956
Final R indexes [all data]	R_1 = 0.1238, wR_2 = 0.2074
Largest diff. peak/hole / e Å^{-3}	1.53/-1.31

Table S2 The crystal structure parameters for **$Pd_1Ag_{14}(P(Ph\text{-}p\text{-}OMe)_3)_7(SPh)_6$ (Pd_1Ag_{14}-E)**.

Empirical formula	$C_{183}H_{177}Ag_{14}O_{21}P_7PdS_6$
Formula weight	4738.19
Temperature/K	170 K
Crystal system	triclinic
Space group	$P\bar{1}$
a/Å	19.457(14)
b/Å	20.805(15)
c/Å	27.840(19)
α/°	82.006(16)
β/°	74.854(18)
γ/°	84.149(17)
Volume/Å^3	10747(13)
Z	2
ρ_{calc}g/cm^3	1.462
μ/mm^{-1}	1.488
F(000)	4684.0
Radiation	Mo Kα (λ = 0.71073)
2Θ range for data collection/°	3.828 to 50
Index ranges	$-23 \le h \le 22$, $-24 \le k \le 24$, $-33 \le l \le 33$
Reflections collected	199172
Independent reflections	37751 [R_{int} = 0.2071, R_{sigma} = 0.1511]
Data/restraints/parameters	37751/3026/1802
Goodness-of-fit on F^2	1.012
Final R indexes [I>=2σ (I)]	R_1 = 0.1045, wR_2 = 0.3055
Final R indexes [all data]	R_1 = 0.1754, wR_2 = 0.3468
Largest diff. peak/hole / e Å^{-3}	2.48/-2.76

Table S3 The atomic ratio of Pd, Ag, S, P, F, and O elements in **Pd_1Ag_{14}-S*** nanocluster was calculated by XPS and EDS measurements.

Pd_1Ag_{14}-S*	**Ag (%)**	**Pd (%)**	**S (%)**	**P (%)**	**F (%)**	**O (%)**
XPS result	22.84	1.65	9.78	13.55	31.46	20.72
EDS result	25.37	1.83	10.37	13.78	28.41	20.24

Table S4 Based on Ag atom (one **Pd_1Ag_{14}-S*** nanocluster contains 14 Ag atoms), the ratio of Ag, F, and O elements in **Pd_1Ag_{14}-S*** nanocluster was calculated by XPS and EDS measurements in Table 3.

Pd_1Ag_{14}-S*	**Ag**	**F**	**O**
XPS result	14	19.3	12.7
EDS result	14	15.7	11.2